Multimodality Imaging of IL-18–Binding Protein-Fc Therapy of Experimental Lung Metastasis

Qizhen Cao,[1] Weibo Cai,[1,2] Gang Niu,[1] Lina He,[1] and Xiaoyuan Chen[1]

Abstract

Purpose: Interleukin (IL)-18 plays important roles in cancer progression and metastasis. The goal of this study is to identify cell lines that are most sensitive to stand alone IL-18–binding protein (IL-18bp)-Fc treatment, to study the pharmacokinetics and tumor targeting efficiency of IL-18bp-Fc, and to evaluate the efficacy of IL-18bp-Fc in treating breast cancer experimental lung metastasis by multimodality imaging.

Experimental Design: Reverse transcription-PCR, ELISA, and other cell-based assays were done on murine 4T1, CT-26, and B16F10 cells. The most IL-18bp-Fc–sensitive 4T1 cells were stably transfected with firefly luciferase (fLuc) and injected i.v. into female BALB/C mice to establish the experimental lung metastasis model. Tumor targeting efficiency and pharmacokinetics of IL-18bp-Fc was assessed by ^{64}Cu-DOTA-IL-18bp-Fc positron emission tomography (PET) and biodistribution studies. Two groups of fLuc-4T1 experimental lung metastasis tumor-bearing mice were each given saline or IL-18bp-Fc (1 mg/kg) daily i.p. Bioluminescence imaging, ^{18}F-FDG PET, and computed tomography scans were done to evaluate the treatment efficacy. *Ex vivo* experiments were also carried out to validate the imaging results.

Results: IL-18bp-Fc had high and specific accumulation in the fLuc-4T1 lung metastasis tumor as evidenced by both PET and biodistribution studies. Bioluminescence imaging, ^{18}F-FDG PET, and computed tomography scans all revealed that IL-18bp-Fc treatment was effective in inhibiting the lung metastasis tumor progression, validated by *ex vivo* examination of the lung.

Conclusions: IL-18bp-Fc therapy can inhibit 4T1 breast cancer experimental lung metastasis. Noninvasive multimodality molecular imaging is a powerful tool for evaluating the tumor targeting efficiency/pharmacokinetics of the drug and effective monitoring of the therapeutic response.

Interleukin (IL)-18, a member of the IL-1 superfamily, is a cytokine produced by macrophages and other cells (1). It plays a central role in inflammation and immune response, contributing to the pathogenesis and pathophysiology of infectious and inflammatory diseases (2, 3). A wide range of normal and cancer cell types can produce and respond to IL-18 through its receptor (IL-18R), a member of the toll-like receptor family (4). Increase of IL-18 concentration in the blood of cancer patients has been associated with disease progression and, in some cancer types, with metastatic recurrence risk as well as poor clinical outcome and survival (5–8). Studies have shown that constitutive or genetically manipulated production of IL-18 can enhance antitumor response and improve survival under experimental conditions (9–11). However, there have also been many reports revealing the activation of cancer progression by IL-18 (12–14). Thus, the role of IL-18 in cancer progression and metastasis remains controversial.

The activity of IL-18 is regulated by IL-18–binding protein (IL-18bp), a 40-kDa glycoprotein that binds and neutralizes IL-18 with high affinity, thereby preventing its interaction with IL-18R (15). Blockade of IL-18 bioactivity by use of IL-18bp is a promising therapeutic approach whenever the risk of infectious complications can be clinically controlled. Because IL-18bp administration has no toxicity and very few side effects, targeting endogenous IL-18 with exogenously administered IL-18bp (or other molecules that bind IL-18) may help dismantling the role of IL-18 in preclinical models of cancer and immunoinflammatory diseases, which may facilitate the use of IL-18bp (or other molecules that bind IL-18) in the clinical setting.

The IL-18bp-Fc fusion protein was generated by joining the entire IL-18bp cDNA to the CH_2 and CH_3 domains of human IgG1 in an expression plasmid. This divalent fusion protein IL-18bp-Fc binds and neutralizes human, mouse, and rat IL-18 with a dissociation constant of 0.3 to 5 nmol/L (16). The high binding affinity and long circulation half-life, two properties that the two components of the IL-18bp-Fc fusion protein

Authors' Affiliations: [1]The Molecular Imaging Program at Stanford, Department of Radiology and Bio-X Program, Stanford University School of Medicine, Stanford, California and [2]Departments of Radiology and Medical Physics, School of Medicine and Public Health, University of Wisconsin - Madison, Madison, Wisconsin
Received 1/5/08; revised 5/14/08; accepted 5/28/08.

Grant support: National Cancer Institute (R01 CA119053, R21 CA121842, R21 CA102123, P50 CA114747, U54 CA119367, and R24 CA93862), the Department of Defense (W81XWH-07-1-0374, W81XWH-04-1-0697, W81XWH-06-1-0665, W81XWH-06-1-0042), Department of Defense PCRP PC073549 (G. Niu), and a Benedict Cassen Postdoctoral Fellowship (W. Cai) from the Education and Research Foundation of the Society of Nuclear Medicine.

The costs of publication of this article were defrayed in part by the payment of page charges. This article must therefore be hereby marked *advertisement* in accordance with 18 U.S.C. Section 1734 solely to indicate this fact.

Requests for reprints: Xiaoyuan Chen, The Molecular Imaging Program at Stanford, Department of Radiology and Bio-X Program, Stanford University School of Medicine, 1201 Welch Road, P095, Stanford, CA 94305-5484. Phone: 650-725-0950; Fax: 650-736-7925; E-mail: shawchen@stanford.edu.

doi:10.1158/1078-0432.CCR-08-0049

Translational Relevance

Interleukin (IL)-18, a member of the IL-1 superfamily, plays a key role in inflammation, immune response, and cancer progression. The activity of IL-18 is regulated by IL-18–binding protein (IL-18bp), a 40-kDa glycoprotein that binds and neutralizes IL-18 with high affinity, thereby preventing its interaction with IL-18R. Blockade of IL-18 bioactivity by use of IL-18bp-Fc fusion protein is a promising anticancer approach. This study shows the effectiveness of IL-18bp-Fc fusion protein in delaying breast cancer lung metastasis, obviated by multimodality molecular imaging techniques such as positron emission tomography, bioluminescence imaging, and computed tomography. The success of this study warrant clinical translation of IL-18bp-Fc fusion protein for cancer therapy and the application of molecular imaging to assess drug targeting efficiency and to monitor therapy response.

could respectively contribute, makes IL-18bp-Fc a promising therapeutic agent. Indeed, the therapeutic efficacy of IL-18bp-Fc has been shown in many disease models (16–18).

Molecular imaging, the visualization, characterization, and measurement of biological processes at the molecular and cellular levels in humans and other living systems (19), has flourished over the last decade. Continued development and wider availability of scanners dedicated to small animal imaging studies (20–22), which can provide a similar *in vivo* imaging capability in rodents, primates, and humans, can enable smooth transfer of knowledge and molecular measurements between species, thereby facilitating clinical translation. Noninvasive molecular imaging can play important roles in early lesion detection, monitoring the therapeutic efficacy, and facilitating drug development, thereby leading to much earlier diagnosis, earlier treatment, and better prognosis, which will eventually enable personalized medicine (23, 24).

The purpose of this study was to identify tumor cells that are most sensitive to IL-18bp-Fc treatment *in vitro*, to understand the pharmacokinetics and tumor targeting efficiency of IL-18bp-Fc using positron emission tomography (PET), and to evaluate the therapeutic efficacy of IL-18bp-Fc by multimodality molecular imaging [PET, bioluminescence imaging (BLI), and computed tomography (CT)]. To the best of our knowledge, this is the first study to noninvasively evaluate the therapeutic efficacy of IL-18bp-Fc in a lung metastasis model with multimodality molecular imaging.

Materials and Methods

Chemicals and reagents. Human recombinant IL-18bp-Fc was a generous gift from Dr. Mizhou Hui (AmProtein Corp., Camarillo, CA). D-Luciferin was purchased from Biosynth International, Inc.

Cell lines. The murine 4T1 breast cancer, CT-26 colorectal cancer, and B16F10 melanoma cell lines were purchased from American Type Culture Collection. The cell lines were maintained in RPMI 1640 (Invitrogen) supplemented with 10% fetal bovine serum at 37°C with 5% CO_2. The cells were used when they reached 70% to 85% confluence.

Reverse transcription-PCR. The mRNA levels of IL-18, IL-18R, IL-1β–converting enzyme (ICE; caspase-1), and β-actin (internal standard) were evaluated by reverse transcription-PCR. Total RNA was isolated from the cell lines using the RNeasy Plus Mini kit (Qiagen). Reverse transcription of total RNA was carried out using the SuperScript III first-strand synthesis system (Promega). The primers used were as follows: murine IL-18, 5′-ggctgccatgtcagaagact-3′ (sense) and 5′-gggttcactggcactttgat-3′ (antisense); murine IL-18R, 5′-cgctgaaactcctgaagtcc-3′ (sense) and 5′-ttgacatcaagctcgtctgg-3′ (antisense); murine ICE, 5′-cacagctctggagatggtga-3′ (sense) and 5′-tctttcaagcttgggcactt-3′ (antisense); murine β-actin, 5′-gctacagcttcaccaccaca-3′ (sense) and 5′-aaggaaggctggaaaagagc-3′ (antisense). PCR was carried out for 30 cycles using the GoTaq green master mix instrument (Promega).

ELISA. 4T1, CT-26, and B16F10 cells were each seeded into 12-well plates with cell culture medium. After incubation for 24 h, the cells were washed with PBS thrice and serum-free medium was added. Twenty-four hours later, the supernatants were collected in which the concentration of functionally active IL-18 was measured using a two-site sandwich ELISA kit (BD Biosciences). The final data were normalized by the amount of total protein of the lysed cell in each well.

Cell proliferation assay and cell migration assay. The 3-(4, 5-dimethylthiazolyl-2)-2, 5-diphenyltetrazolium bromide (MTT; American Type Culture Collection) assay measures the cell proliferation rate. Ten thousand tumor cells were seeded per well in a 96-well plate and allowed to incubate for 16 h. After incubation with various concentrations of IL-18bp-Fc for 48 h, 10 μL of MTT reagent were added to each well. Four hours later, when the purple precipitate became visible, 100 μL of detergent reagent were added to each well and the plate was left in the dark for 2 h at room temperature. The absorbance at 570 nm was then measured using a plate reader.

For cell migration assay, 4T1 cells were seeded in 6-well plates at a density of 5×10^5 cells per well in culture medium. Twenty-four hours later, the confluent monolayer of culture was scratched with a fine pipette tip. The wells were washed thrice with PBS to remove the floating cells. Cell culture medium with various concentrations of IL-18bp-Fc (0, 0.5, 5, and 50 μg/mL) was then added to each well. Twenty hours later, the wells were examined under a microscope.

Stable transfection of firefly luciferase. Transfection was done with pcDNA 3.1 cytomegalovirus-firefly luciferase (fLuc) DNA and Lipofectamine 2000 (Invitrogen) using 80% confluent 4T1 cells. The cells were incubated for 48 h before the culture medium was changed. Selection was made by adding selective medium containing 1 mg/mL G418 antibiotic (Stemcell Technologies, Inc.) every 2 to 3 d. Two weeks later, the cells were analyzed and subcloned in 24-well plates. When reaching 80% confluence, the cells in the plate were imaged under a cooled CCD camera (Caliper Life Sciences;) after addition of the substrate D-luciferin (20 μL per well of 3 mg/mL stock). The selected clones were trypsinized, subcultured, lysed, and assayed by luminometry for fLuc activity. The clone with the highest fLuc activity (fLuc-4T1) was selected for further studies. The fLuc-4T1 and 4T1 cells were compared using the abovementioned assays and no significant difference was observed (data not shown).

Experimental lung metastasis model and treatment protocol. All animal procedures were done according to a protocol approved by Stanford University Institutional Animal Care and Use Committee. The fLuc-4T1 breast cancer experimental lung metastasis model was established by i.v. injection of 1×10^5 fLuc-4T1 cells in 100 μL of PBS into 6-wk-old female BALB/C mice (Harlan). For treatment, IL-18bp-Fc was administered i.p. everyday at a dose of 1 mg/kg starting from the day of tumor inoculation.

BLI. BLI was done using the IVIS200 system (Caliper Life Sciences). Mice were anesthetized with 2% isoflurane in O_2 and received i.p. injection of D-luciferin solution in PBS at a dose of 150 mg/kg. Serial images were acquired at 5 to 20 min after D-luciferin administration (integration, 30 s; binning, 4 s). The BLI signal intensity was quantified

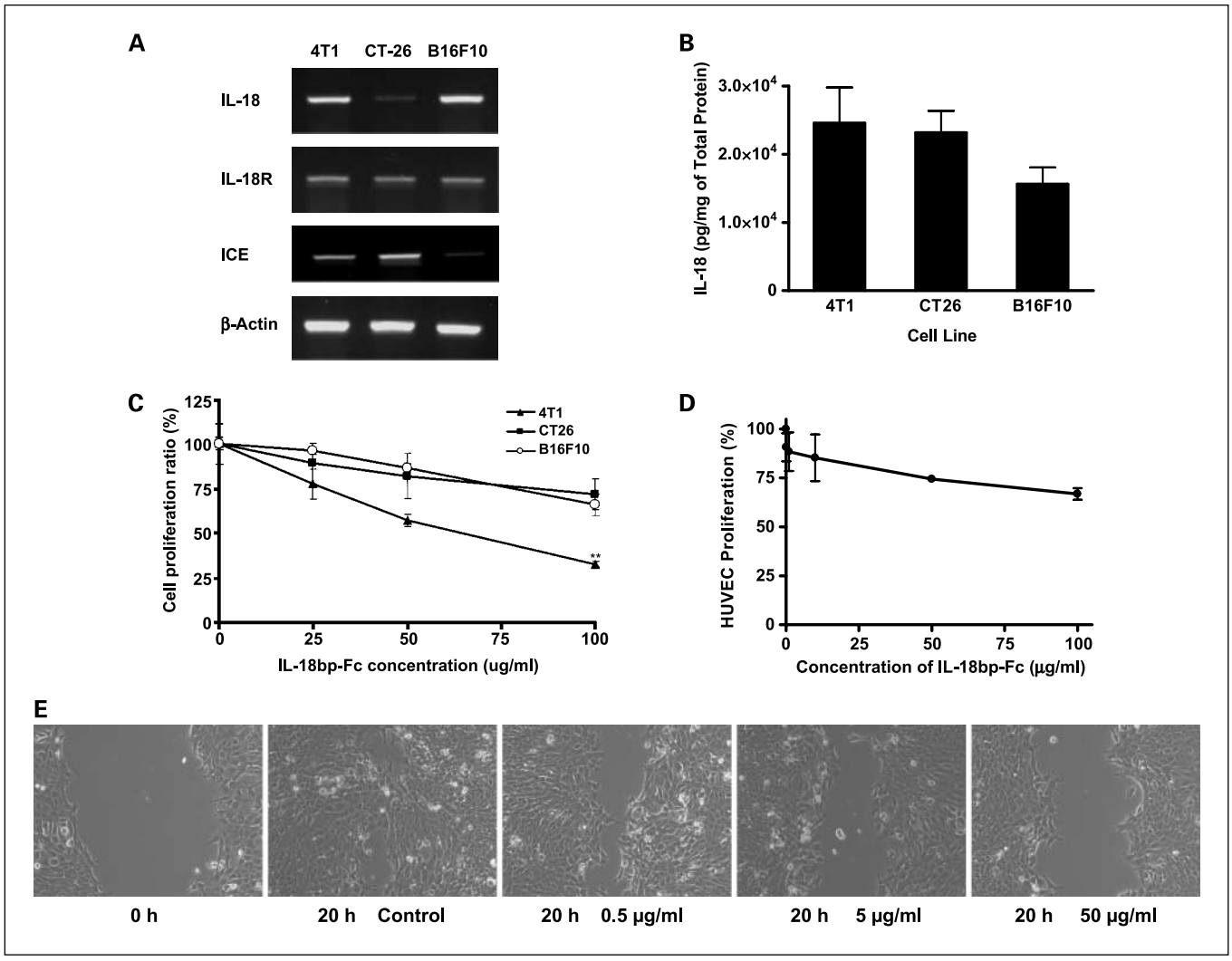

Fig. 1. Evaluating the effect of IL-18bp-Fc on murine 4T1 breast cancer, CT-26 colorectal cancer, and B16F10 melanoma cell lines *in vitro*. *A,* reverse transcription-PCR of IL-18, IL-18R, and ICE (caspase-1) in the three cell lines. β-Actin was used as an internal standard. *B,* ELISA measurement of secreted bioactive IL-18 in the cell culture medium. The data were normalized to the amount of total protein in the lysed cells. $n = 3$. *C,* the effect on 4T1, CT-26, and B16F10 tumor cell proliferation after incubation with various concentrations of IL-18bp-Fc for 48 h at 37°C. $n = 4$. **, $P < 0.01$. *D,* the effect on human umbilical vein endothelial cell (HUVEC) proliferation after incubation with various concentrations of IL-18bp-Fc for 48 h at 37°C. $n = 4$. *E,* the effect on 4T1 cell migration after incubation with various concentrations of IL-18bp-Fc for 20 h at 37°C.

as the sum of all detected photon counts within the region of interest after subtraction of background luminescence.

1,4,7,10-tetra-azacylododecane conjugation and ^{64}Cu-labeling. Detailed procedures for 1,4,7,10-tetra-azacylododecane (DOTA) conjugation and ^{64}Cu-labeling have been reported earlier (25, 26). $^{64}CuCl_2$ (1 mCi) was diluted in 300 μL of 0.1 mol/L sodium acetate buffer (pH 6.5) and added to 30 μg of DOTA-IL-18bp-Fc. The reaction mixture was incubated for 1 h at 40°C with constant shaking. ^{64}Cu-DOTA-IL-18bp-Fc was then purified by size exclusion chromatography (PD-10 column; GE Healthcare) using PBS as the mobile phase.

MicroPET imaging. PET imaging of fLuc-4T1 tumor-bearing mice was done on a microPET R4 rodent model scanner (Siemens Medical Solutions) as described earlier (27, 28). Each mouse was anesthetized and injected with ~100 to 300 μCi of ^{64}Cu-DOTA-IL-18bp-Fc or ^{18}F-FDG via tail vein and scanned at various time points postinjection (p.i.). For each microPET scan, three-dimensional region of interests were drawn over the whole lung and other major organs on decay-corrected whole-body coronal images. The average radioactivity concentration in the region of interest was obtained from mean pixel values within the region of interest volume, which was converted to counts per milliliter per minute by using a predetermined conversion factor. The results were then divided by the injected dose to obtain an image region of interest–derived percentage injected dose per cubic centimeter of tissue (%ID/cm^3).

Biodistribution studies. Normal BALB/C mice or fLuc-4T1 lung metastasis mice were injected with ~10 μCi of ^{64}Cu-DOTA-IL-18bp-Fc via the tail vein and were euthanized at 4 and 48 h p.i. Blood, lung, major organs, and tissues were collected, wet-weighed, and counted in a γ-counter (Packard). The results were normalized to 20 grams of mouse body weight and reported as mean %ID/g ± SD except for the lung, which was presented as mean %ID/organ ± SD ($n = 3$ per group).

MicroCT imaging. MicroCT scans were carried out on a small-animal CT scanner without gating (GE Healthcare). Mice were anesthetized with isoflurane during the scans and the CT images were reconstructed using filtered back-projection and analyzed using the vendor software (MicroView; GE Healthcare).

H&E staining. At the end of the study, the whole lung of each mouse was harvested and fixed in 100 mL of buffered formalin for 24 h. H&E staining was carried out, and the metastatic nodules in the

lung tissue were counted under a microscope (magnification, ×16; $n = 3$ per group).

Statistical analysis. Statistical significance was determined by one-way ANOVA. P values of <0.05 were considered statistically significant.

Results

Expression level of IL-18, IL-18R, and ICE in different cell lines. IL-18 is converted from an inactive form (24 kDa) to a bioactive form (18 kDa) upon cleavage by ICE, which was then secreted (29, 30). Three murine cell lines, 4T1 breast cancer, CT-26 colorectal cancer, and B16F10 melanoma were tested in this study. Reverse transcription-PCR experiments (Fig. 1A) revealed similar IL-18R expression level in all three cell lines, whereas the level of IL-18 was quite different. 4T1 and B16F10 cells both had much higher IL-18 expression than CT-26 cells. Interestingly, the ICE level follows the order of CT-26 > 4T1 > B16F10. Because reverse transcription-PCR measures the level of inactive form of IL-18 (24 kDa), ELISA experiments were also carried out to measure the amount of active IL-18 (18 kDa) secreted into the cell culture medium (Fig. 1B). Based on ELISA, both CT-26 and 4T1 cells had higher IL-18 level than B16F10 cells, which corroborates with the ICE expression level. Taken together, 4T1 cells have high expression of inactive IL-18 and medium level of ICE, which gives high level of secreted active IL-18; CT-26 cells have low expression of inactive IL-18 and high level of ICE, which also yields high level of secreted active IL-18; B16F10 cells have high level of inactive IL-18 and low level of ICE, which leads to relatively lower level of secreted active IL-18.

***Effect of IL-18bp-Fc* in vitro.** Next, we investigated the effect of IL-18bp-Fc on the proliferation of these cells. Incubation with IL-18bp-Fc for 48 hours inhibited the proliferation of all 3 cells in a dose-dependent manner (Fig. 1C). Comparing the 3 cell lines, 4T1 cells are most sensitive to stand alone IL-18bp-Fc treatment, which had ~70% inhibition in cell proliferation at the dose of 100 μg/mL, significantly more than either CT-26 or B16F10 cells (29% ± 6% and 34% ± 8%, respectively; $n = 4$; $P < 0.01$ in both cases). These results correlate well with the active IL-18 expression level in that the cell line with the highest IL-18 expression (4T1) is the most sensitive to stand alone IL-18bp-Fc treatment.

Additional experiments also revealed that incubation with IL-18bp-Fc inhibited the proliferation of human umbilical vein endothelial cells (American Type Culture Collection) and the migration of 4T1 cells in a dose-dependent manner (Fig. 1D and E). Based on these results, we chose the 4T1 breast cancer experimental lung metastasis model for IL-18bp-Fc therapy.

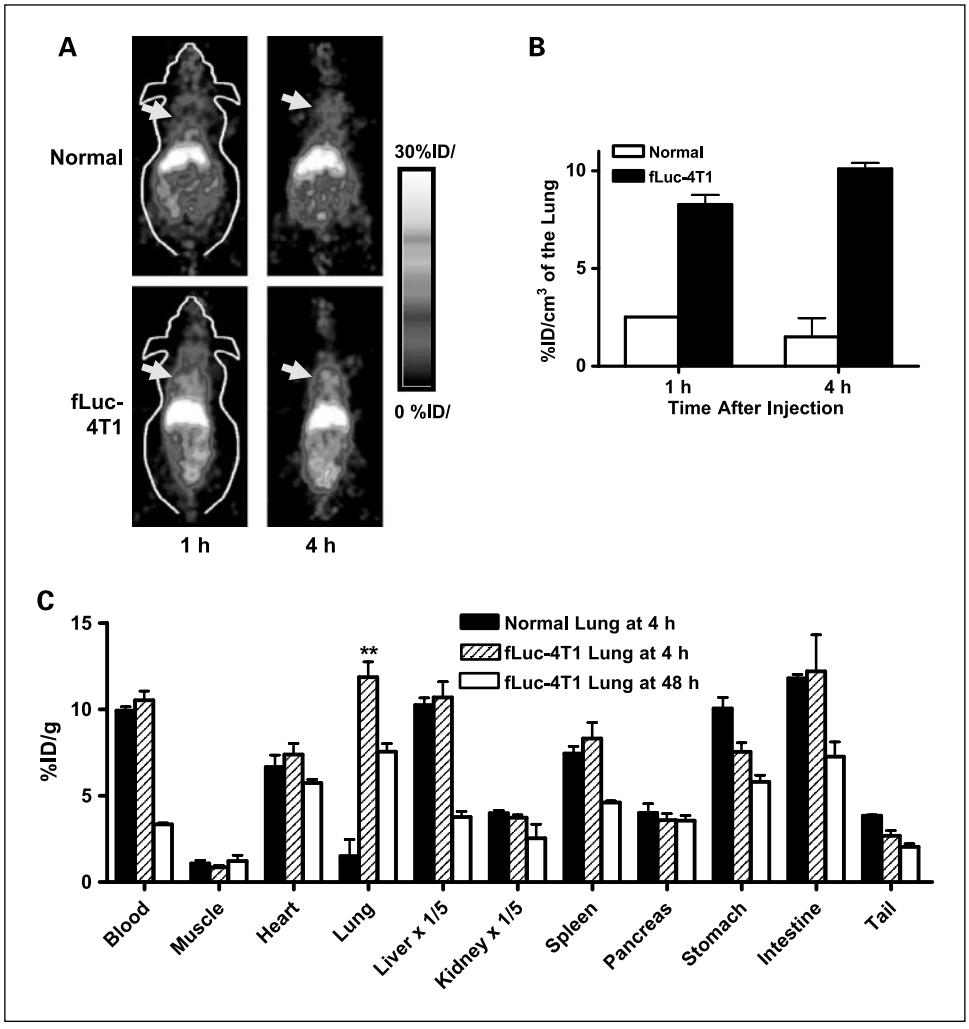

Fig. 2. MicroPET and biodistribution studies of ^{64}Cu-DOTA-IL-18bp-Fc. *A,* coronal microPET images of normal and fLuc-4T1 lung metastasis tumor-bearing mice at 1 and 4 h after injection of ^{64}Cu-DOTA-IL-18bp-Fc. *Arrows,* the lung. *B,* lung uptake of ^{64}Cu-DOTA-IL-18bp-Fc in normal mice and fLuc-4T1 lung metastasis tumor-bearing mice based on microPET scans. *C,* biodistribution of ^{64}Cu-DOTA-IL-18bp-Fc in normal and fLuc-4T1 lung metastasis tumor-bearing mice at 4 and 48 h after injection. Note that the lung uptake was presented as %ID/organ, whereas tracer uptake in all other organs were presented as %ID/g. $n = 3$; **, $P < 0.01$.

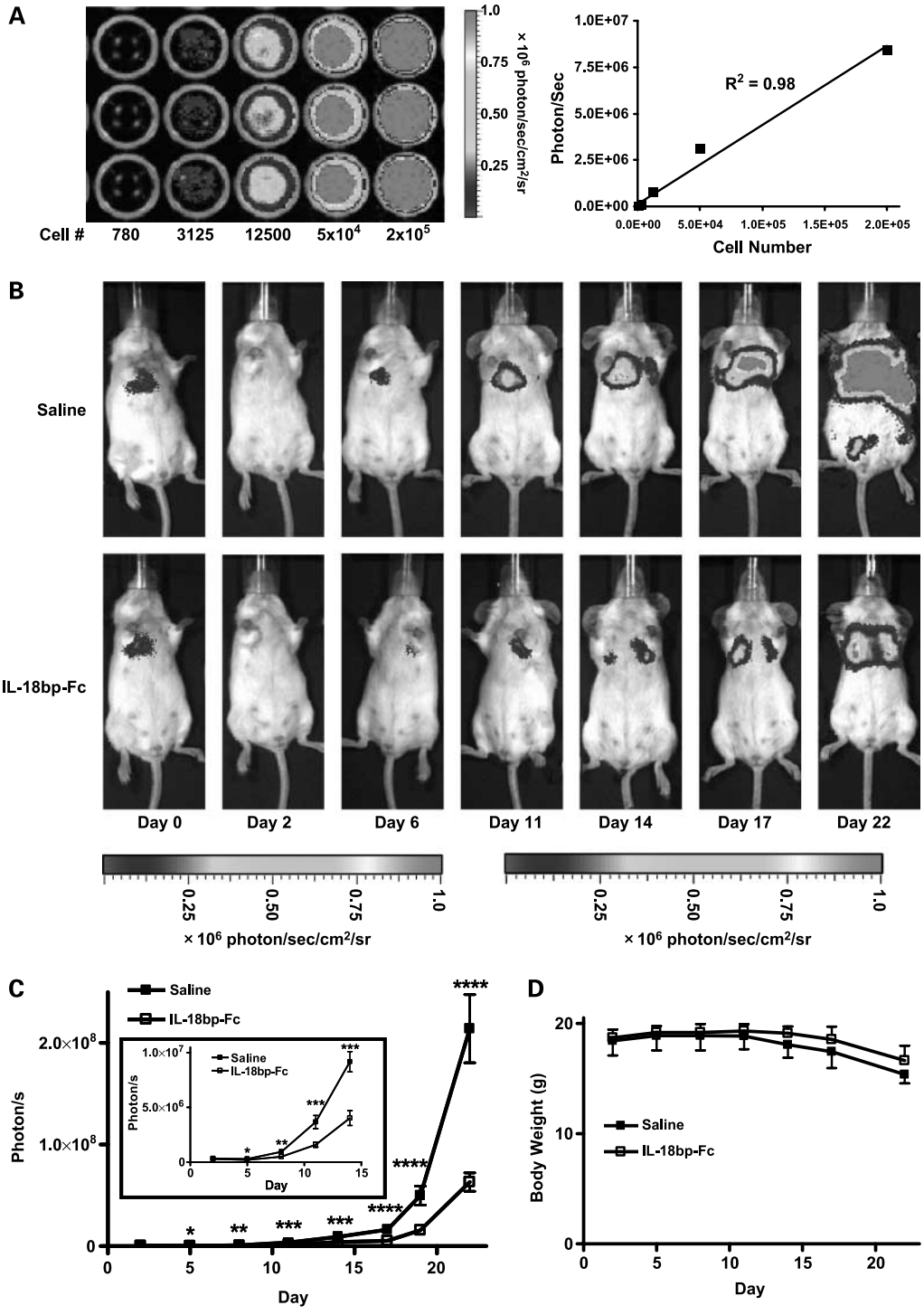

Fig. 3. BLI to monitor the therapeutic response. *A,* bioluminescence signal of fLuc-4T1 cells has a linear correlation with the cell number ($R^2 = 0.98$). *B,* serial bioluminescence images of fLuc-4T1 lung metastasis tumor-bearing mice underwent saline or IL-18bp-Fc treatment. *C,* total photon flux of the BLI signal from the lung of the two groups. *Inset,* data between day 0 and day 14. *D,* average body weight of the two groups of animals. $n = 9$ per group except at day 22 ($n = 7$ for the saline group because 2 animals died). *, $P < 0.05$; **, $P < 0.01$; ***, $P < 0.001$; ****, $P < 0.0001$.

The 4T1 cells were stably transfected with fLuc so that the therapeutic effect can be noninvasively monitored by BLI.

MicroPET imaging using ^{64}**Cu-*DOTA-IL-18bp-Fc.*** Before the treatment study, we evaluated the pharmacokinetics and tumor targeting efficiency of IL-18bp-Fc *in vivo* by PET imaging. There are 2.5 ± 0.1 DOTA molecules per IL-18bp-Fc ($n = 4$) and the ^{64}Cu-labeling yield was 21.1% ± 1.2% ($n = 3$). The coronal PET images of both normal and fLuc-4T1 tumor-bearing mice

at 1 and 4 hours p.i. are shown in Fig. 2A. The lung uptake of ^{64}Cu-DOTA-IL-18bp-Fc was much higher in the fLuc-4T1 tumor-bearing lung (8.3%ID/cm^3 ± 0.5%ID/cm^3 and 10.1%ID/cm^3 ± 0.3%ID/cm^3 at 1 and 4 hours p.i., respectively; n = 3) than in the lung of normal mice (2.5%ID/cm^3 and 1.5%ID/cm^3 ± 1.0%ID/cm^3 at 1 and 4 hours p.i., respectively; Fig. 2B). Note that the liver uptake of ^{64}Cu-DOTA-IL-18bp-Fc was also prominent, due to the hepatic clearance of the tracer and possibly some *trans*-chelation of ^{64}Cu.

Biodistribution of ^{64}Cu-DOTA-IL-18bp-Fc. Biodistribution of ^{64}Cu-DOTA-IL-18bp-Fc in normal and fLuc-4T1 tumor-bearing mice were carried out at 4 and 48 hours p.i. (Fig. 2C). Tracer distribution was presented as %ID/organ for the lung and %ID/g for all other major organs. Lung tissue, blood, and air determine the physical density of the lung. These components are not homogeneously distributed throughout the lungs, and their relative proportion changes continuously during respiration. The lung density of dead animal devoid of air in the lung is significantly higher than that of the breathing live animals. We thus used the unit of %ID/organ for the lung to correlate the noninvasive PET imaging and *ex vivo* direct tissue sampling. The uptake of ^{64}Cu-DOTA-IL-18bp-Fc was significantly higher in the fLuc-4T1 lung than in the normal lung (11.9%ID/organ ± 0.9%ID/organ and 1.5%ID/organ ± 1.0%ID/organ at 4 hours p.i., respectively; n = 3; $P < 0.01$). The slow clearance of the tracer uptake from the lung (7.6%ID/organ ± 0.5%ID/organ remaining at 48 hours p.i.) confirmed the specific binding *in vivo*. Comparing the PET and biodistribution data at 4 hours p.i., the uptake in all organs were comparable suggesting that quantitative analysis of PET scans is truly reflecting the tracer distribution *in vivo*.

There was no significant difference of ^{64}Cu-DOTA-IL-18bp-Fc distribution in any other organ (besides the lung) between normal mice and fLuc-4T1 tumor-bearing mice. For the tumor-bearing mice, the initial liver uptake of ^{64}Cu-DOTA-IL-18bp-Fc was high (53.5%ID/g ± 0.9%ID/g at 4 hours p.i.) and dropped to 18.9%ID/g ± 1.6%ID/g at 48 hours p.i.; The kidney uptake was 18.9%ID/g ± 0.2%ID/g and 12.7%ID/g ± 0.8%ID/g at 4 and 48 hours p.i., respectively; The tracer uptake in most other organs are relatively low. Because the blood concentration of ^{64}Cu-DOTA-IL-18bp-Fc dropped significantly from 10.5%ID/g ± 0.5%ID/g at 4 hours p.i. to 3.4%ID/g ± 0.1%ID/g at 48 hours p.i., we chose to administer IL-18bp-Fc everyday to maintain the serum level of IL-18bp-Fc to achieve optimal therapeutic effect.

BLI to monitor the treatment efficacy. No significant difference between 4T1 and fLuc-4T1 cells was observed in terms of proliferation, IL-18 expression, tumorigenicity, or migration (data not shown). To confirm that the level of reporter gene activity correlated with the number of cells, different numbers of fLuc-4T1 cells (8×10^2 to 5×10^5) were assayed for fLuc enzyme activity. A robust linear correlation between the cell number and fLuc activity was observed (R^2 = 0.98; Fig. 3A). Two groups of mice (n = 9 per group) were subjected to i.p. injection of either saline or IL-18bp-Fc daily. Various studies have shown that BLI can provide rapid, noninvasive, quantitative, and sensitive monitoring of tumor growth and regression in animal tumor models (31–33). Thus, BLI was done every 3 days to monitor the progression of fLuc-4T1 lung tumor burden. Following i.v. injection, the presence of fLuc-4T1 cells in the lung can be clearly detected upon i.p. injection of D-luciferin. After initial decrease over the first several days after injection, the BLI signal of the mice injected with saline increased exponentially and became significantly different from the IL-18bp-Fc–treated group from day 5 onwards (Fig. 3B and C). IL-18bp-Fc clearly inhibited the tumor growth *in vivo*, although it was not able to completely ablate the tumor progression. At late time points (after day 14), the average body weight of the animals began to drop in both groups due to increased lung tumor burden, which caused respiratory difficulty and other symptoms (Fig. 3D), with much less body weight loss in the IL-18bp-Fc group than the saline group. On day 17, the average BLI signal of the IL-18bp-Fc group was <33% of that of the saline group ($P < 0.0001$). At this point, the animals in the saline group began to die, and at day 22, 2 of 9 animals died in the saline group, whereas all animals in the IL-18bp-Fc group survived. In summary, BLI was successful in noninvasively monitoring the treatment efficacy of IL-18bp-Fc in the fLuc-4T1 breast cancer experimental lung metastasis model.

^{18}F-FDG PET to monitor the treatment efficacy. ^{18}F-FDG PET has been routinely used in both clinical and preclinical studies to evaluate the stage of tumor progression and the efficacy of therapeutic intervention by measuring the glucose metabolism (34). We carried out ^{18}F-FDG microPET scans at day 17 after IL-18bp-Fc treatment. The heart had prominent uptake of ^{18}F-FDG due to the constant beating, which has high demand for glucose. The lung of normal mice (no tumor present) had minimum uptake of ^{18}F-FDG (1.7%ID/cm^3 ± 0.1%ID/cm^3; n = 3; Fig. 4A and B). Both the saline group and the IL-18bp-Fc treatment group had significantly higher ^{18}F-FDG lung uptake than the normal lung ($P < 0.01$). Most importantly, the tracer uptake in the IL-18bp-Fc–treated lung was significantly lower

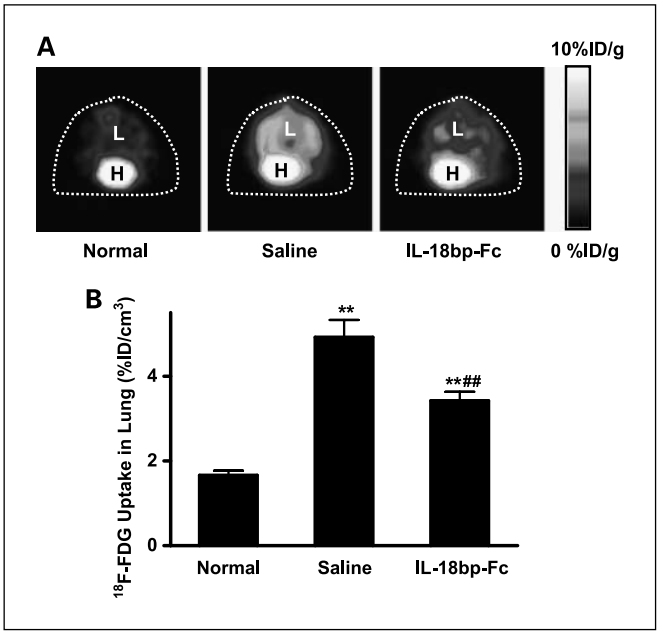

Fig. 4. ^{18}F-FDG PET to monitor the therapeutic response. *A,* transaxial microPET images of normal (no tumor present), saline-treated, and IL-18bp-Fc–treated fLuc-4T1 lung metastasis tumor-bearing mice (day 17) at 1 h after i.v. ^{18}F-FDG injection. *H,* heart; *L,* lung. *B,* lung uptake of ^{18}F-FDG in different groups. **, $P < 0.01$ compared with normal mice; ##, $P < 0.01$ compared with saline-treated mice. n = 3.

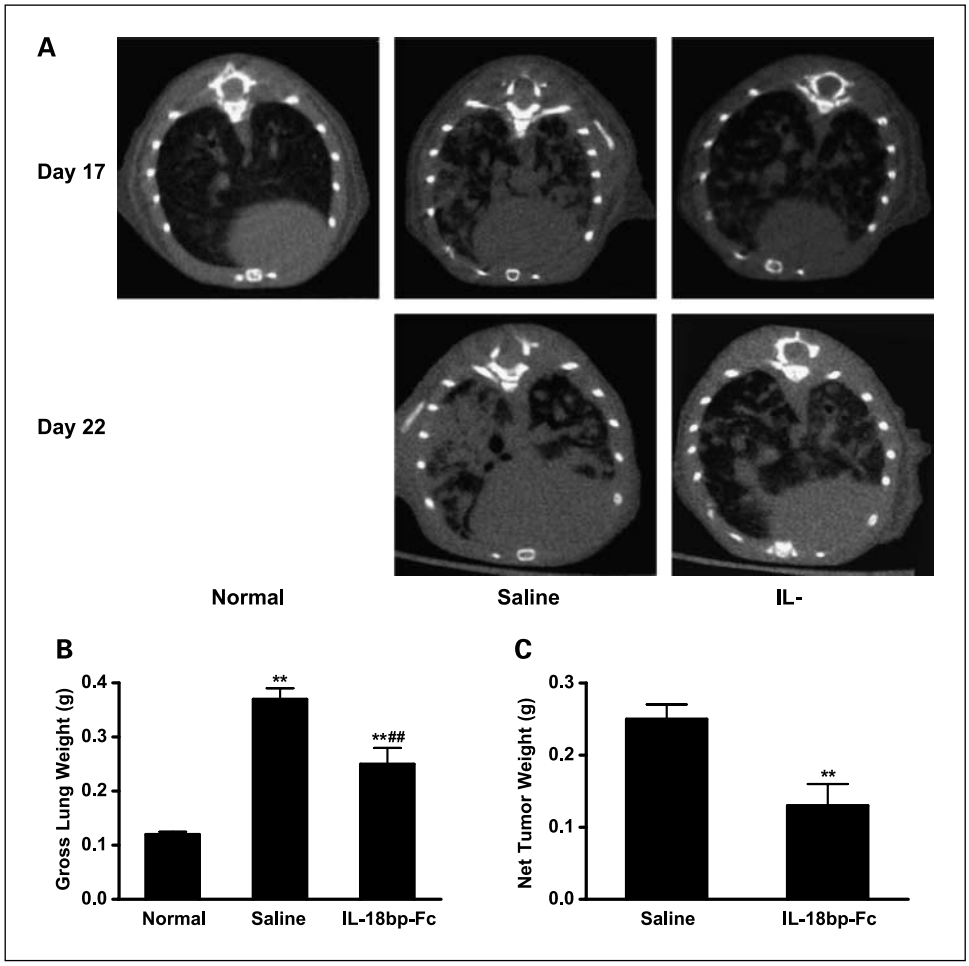

Fig. 5. MicroCT imaging to monitor the therapeutic response and *ex vivo* examination of the lung. *A,* MicroCT images of the normal (no tumor present), saline-treated, and IL-18bp-Fc – treated fLuc-4T1 lung metastasis tumor-bearing mice at day 17 and day 22. Images are representative of three animals per group. *B,* average lung weight of normal (no tumor present), saline-treated, and IL-18bp-Fc – treated fLuc-4T1 lung metastasis tumor-bearing mice at day 22. **, $P < 0.01$ compared with normal mice; ##, $P < 0.01$ compared with saline-treated mice. $n = 3$. *C,* "Net" fLuc-4T1 lung tumor weight of the two groups of animals after subtraction of the normal lung weight. **, $P < 0.01$. $n = 3$.

than that of the saline-treated lung (3.4%ID/cm^3 ± 0.2%ID/cm^3 versus 4.9%ID/cm^3 ± 0.4%ID/cm^3; $n = 3$; $P < 0.01$; Fig. 4A and B). Clearly, ^{18}F-FDG PET was able to detect the difference in experimental lung metastasis tumor burden between the two groups during treatment.

MicroCT imaging to monitor the treatment efficacy. Besides BLI and ^{18}F-FDG PET scans, which are evaluating the therapeutic efficacy at the molecular level, we also carried out CT imaging to see whether there is observable difference in overall lung tumor burden. CT scans were done on day 17 and day 22 (Fig. 5A). MicroCT clearly delineated the three-dimensional trabecular microarchitecture *in vivo*. In the CT images of normal lung, only the bronchitis and large vessels can be seen. At day 17, there is some difference between the saline and IL-18bp-Fc–treated group; however, the difference is not very obvious. At day 22, the difference was clearly observable where the lung tumor burden in the saline-treated group was very heavy. The saline-treated mice had increased lung tumor colonization (high density area) involving most of the lung, whereas the tumor burden lung of IL-18bp-Fc–treated mice exhibited lower tissue density, smaller tumor nodules, and less tumor colonization. Overall, CT imaging is not as sensitive as BLI or ^{18}F-FDG PET in monitoring the therapeutic efficacy, although it was able to detect the difference when the tumor burden was dramatically different at late time points.

Lung weight and H&E staining. At the end of IL-18bp-Fc therapy and multimodality imaging, the mice were sacrificed and the whole lung of each mouse was collected and wet weighted (Fig. 5B). The fLuc-4T1 tumor burden lung (saline or IL-18bp-Fc treated) were significantly heavier than the normal lung ($P < 0.01$) because on day 22, the BLI signal of both groups were quite strong. Comparing the two groups, the gross lung weight of IL-18bp-Fc–treated mice was significantly less than the saline-treated mice (0.25 ± 0.03 grams versus 0.37 ± 0.02 grams; $n = 9$; $P < 0.01$), corroborating with the BLI, ^{18}F-FDG, and CT imaging results. The "net" tumor weight (subtracting the weight of the normal lung from that of the tumor burden lung) was also significantly different between the two groups (0.13 ± 0.03 grams versus 0.25 ± 0.02 grams; Fig. 5C; $n = 9$; $P < 0.01$).

H&E staining of the lung tissue sections revealed that IL-18bp-Fc treatment significantly reduced the size and number of metastatic tumor nodules in the mouse lung compared with those of the control group (Fig. 6A and B). The tumor nodules are widely spread through out the lung in the saline-treated group (89.7 ± 11.4 nodules per lung; $n = 3$), whereas there are only sporadic tumor nodules in the IL-18bp-Fc–treated lung (28.3 ± 7.0 nodules per lung; $n = 4$; Fig. 6B). Taken together, *ex vivo* examination of the lung tissue confirmed the therapeutic efficacy of IL-18bp-Fc against experimental lung metastasis, corroborating the findings based on *in vivo* multimodality imaging.

Discussion

Rodent tumor models have become indispensable in the discovery and assessment of new anticancer therapies (35). Many preclinical studies of experimental therapeutics use subcutaneous tumor models, established by injecting rapidly growing mouse or human tumor cell lines in syngeneic or immuno-deficient rodents, to facilitate the quantitation of tumor growth and therapeutic response by measuring the tumor volume. However, these studies may not be relevant to the biological processes occurring during tumor progression. Metastasis is a malignant feature of cancer and a large body of research has revealed that formation of metastasis is a complex and multistep process (36, 37). For a tumor cell to metastasize, it must detach from the primary lesion and invade the surrounding tissue, intravasate into the circulation system, avoid host immune defenses, arrest at a distant site, extravasate, and proliferate. The experimental lung metastasis model used in this study can simulate some of these processes. However, quantitative measurement of therapeutic-induced changes in tumor growth in experiment lung metastasis model is difficult to achieve using traditional approaches, which usually requires large numbers of animals to be sacrificed at multiple time points to overcome the variability between animals. These facts underscore the importance of using imaging tools to non-invasively monitor the therapeutic response to anticancer pharmaceuticals (38, 39). The goal of this study is 3-fold: First, to identify tumor cells that are most sensitive to IL-18bp-Fc treatment based on *in vitro* studies; Second, to study the pharmacokinetics and tumor targeting efficiency of IL-18bp-Fc; Third, to evaluate whether IL-18bp-Fc can inhibit the progression of breast cancer experimental lung metastasis *in vivo* by using multimodality imaging (BLI, PET, and CT).

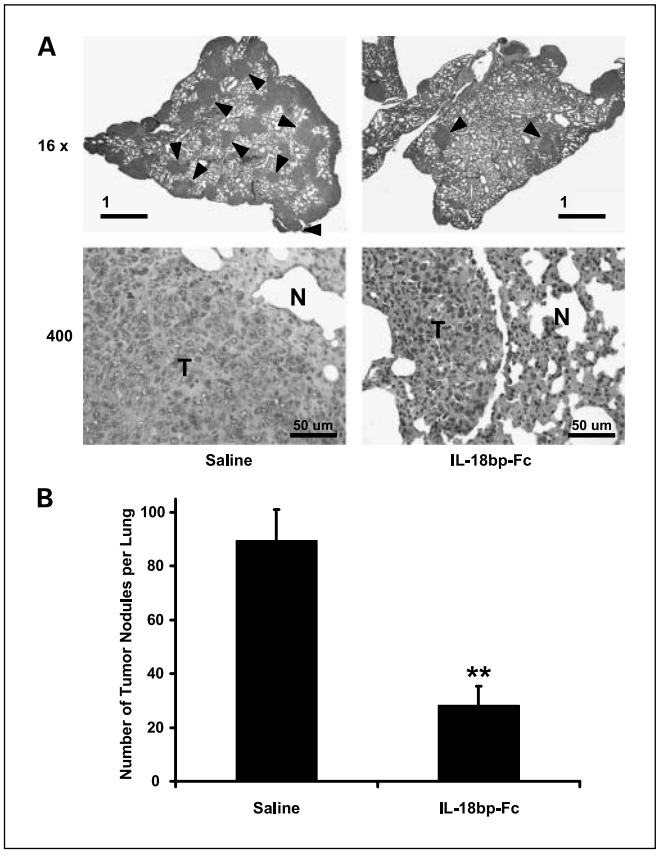

Fig. 6. H&E staining of lung tissue slices. *A,* H&E images of lung tissue slices from the two groups of animals. *Arrowheads,* representative tumor nodules. *T,* tumor; *N,* normal lung tissue. *B,* the average number of tumor nodules per lung for the two groups of animals. **, $P < 0.01$. $n = 3$.

These goals were successfully achieved. Reverse transcription-PCR, ELISA, cell proliferation assay, and cell migration assay identified that 4T1 breast cancer cells are the most sensitive to IL-18bp-Fc treatment *in vitro*. Before initiation of treatment, microPET imaging with ^{64}Cu-labeled IL-18bp-Fc showed the tumor targeting efficiency and facilitated the determination of dose interval. Such study with a radiolabeled drug clearly showed the power of molecular imaging, where cancer patients can also be selected for molecular cancer therapy based on pretreatment screening using a radiolabeled drug (analogue). During and after treatment, the therapeutic efficacy of IL-18bp-Fc was confirmed and successfully monitored by multimodality imaging using BLI, ^{18}F-FDG PET, and CT, all of which were in good agreement with the *ex vivo* examination of the lung. Overall, this study suggested that future clinical multimodality imaging and therapy with agents such as IL-18bp-Fc may provide an effective means to prospectively identify patients who will benefit from such molecular therapy and then stratify, personalize, and monitor treatment to obtain optimal clinical outcomes.

The IL-18bp-Fc used in this study can bind human, mouse, and rat IL-18 with high affinity (16). Therapeutic efficacy of IL-18bp-Fc has been shown in many disease models by other research groups (16–18, 40). Based on our *in vitro, ex vivo*, and multimodality imaging studies, the therapeutic effect of IL-18bp-Fc are likely attributed to the following factors: 4T1 cells express the highest level of bioactive IL-18 therefore are sensitive to IL-18bp-Fc treatment; IL-18bp-Fc had high and specific accumulation in fLuc-4T1 tumor burden lung; Daily administration maintained the blood concentration of the IL-18bp-Fc, which ensures constant supply of the drug to the tumor-bearing lung; IL-18bp-Fc can reduce the expression of vascular cell adhesion molecule-1 (12), which mediates the tumor cell adhesion during the metastatic process; Inhibition of vascular endothelial cell proliferation (Fig. 1D) may lead to inhibition of tumor progression by limiting the blood supply to fLuc-4T1 tumor cells; IL-18 has been reported to have proangiogenic effects (14), therefore IL-18bp-Fc may be able to inhibit angiogenesis and metastasis through IL-18 binding.

There are some limits to this study. Fc receptor is expressed on the surface of certain cells—including natural killer cells, macrophages, neutrophils, and mast cells—that contribute to the protective functions of the immune system. As we used immuocompetent mice to evaluate the treatment efficacy of IL-18bp-Fc, we cannot exclude the possible effect of xeno-immune reaction of Fc besides the stut down of autocrine and paracrine effect of IL-18. Further studies in immunodeficient severe combined immunodeficient or nude mice will help elucidate which mechanism is responsible for the *in vivo* therapeutic effect.

Many imaging techniques have been routinely used in the drug discovery process to directly monitor the drug in blood, normal, and tumor tissues, and to evaluate the effects of the drug in the context of tumor (38, 39). However, with the recent shift in drug discovery from conventional cytotoxic drugs to

novel agents against specific molecular targets, conventional imaging modalities are usually no longer adequate for effective measurement of the therapeutic response. Molecular imaging techniques will play a pivotal role in future cancer management and personalized molecular medicine. In this study, we found that BLI and ^{18}F-FDG PET can detect the therapeutic response earlier than the anatomic imaging techniques such as CT. For BLI, the total photon flux (photon/s) from the whole thorax was significantly different between the two groups as early as day 5 after treatment. For PET, A marked reduction of ^{18}F-FDG activity in the lung was noted for the IL-18bp-Fc – treated group. After subtracting the normal lung background uptake, ^{18}F-FDG uptake in the fLuc-4T1 tumor-bearing lung after IL-18bp-Fc therapy decreased 46% comparing with the saline-treated group. CT is an important tool for providing the anatomical information. However, high-resolution CT imaging requires longer acquisition times, which results in considerable radiation exposure of the animals ($\sim$0.6 Gy per scan; 5% of the LD_{50} for mice). The CT images of the lung between the 2 groups at day 17 after treatment were somewhat different but not very obvious. The difference at day 22 was much more dramatic, confirming the therapeutic efficacy of IL-18bp-Fc. However, accurate quantification of the CT images was rather difficult compared with BLI or PET scans.

In conclusion, IL-18bp-Fc therapy can inhibit breast cancer experimental lung metastasis in animal models. Molecular imaging can play important roles before, during, and after treatment such as evaluating the tumor targeting efficiency of the drug, investigating its pharmacokinetics, and providing noninvasive, accurate, reliable, and more statistically relevant monitoring of the therapeutic response.

Disclosure of Potential Conflicts of Interest

No potential conflicts of interest were disclosed.

Acknowledgments

We thank Dr. Mizhou Hui from AmProtein Corp. for providing the IL-18bp-Fc fusion protein, the cyclotron team at the University of Wisconsin-Madison for ^{64}Cu production, and the cyclotron team at Stanford University for ^{18}F-FDG production.

References

1. Ghayur T, Banerjee S, Hugunin M, et al. Caspase-1 processes IFN-γ-inducing factor and regulates LPS-induced IFN-γ production. Nature 1997;386:619–23.
2. Dinarello CA. Interleukin-18 and the pathogenesis of inflammatory diseases. Semin Nephrol 2007;27:98–114.
3. Reddy P. Interleukin-18: recent advances. Curr Opin Hematol 2004;11:405–10.
4. Sergi B, Penttila I. Interleukin 18 receptor. J Biol Regul Homeost Agents 2004;18:55–61.
5. Eissa SA, Zaki SA, El-Maghraby SM, Kadry DY. Importance of serum IL-18 and RANTES as markers for breast carcinoma progression. J Egypt Natl Cancer Inst 2005;17:51–5.
6. Gunel N, Coskun U, Sancak B, et al. Prognostic value of serum IL-18 and nitric oxide activity in breast cancer patients at operable stage. Am J Clin Oncol 2003;26:416–21.
7. Tsuboi K, Miyazaki T, Nakajima M, et al. Serum interleukin-12 and interleukin-18 levels as a tumor marker in patients with esophageal carcinoma. Cancer Lett 2004;205:207–14.
8. Vidal-Vanaclocha F, Mendoza L, Telleria N, et al. Clinical and experimental approaches to the pathophysiology of interleukin-18 in cancer progression. Cancer Metastasis Rev 2006;25:417–34.
9. Osaki T, Hashimoto W, Gambotto A, et al. Potent antitumor effects mediated by local expression of the mature form of the interferon-γ inducing factor, interleukin-18 (IL-18). Gene Ther 1999;6:808–15.
10. Ju DW, Tao Q, Lou G, et al. Interleukin 18 transfection enhances antitumor immunity induced by dendritic cell-tumor cell conjugates. Cancer Res 2001;61:3735–40.
11. Tatsumi T, Gambotto A, Robbins PD, Storkus WJ. Interleukin 18 gene transfer expands the repertoire of antitumor Th1-type immunity elicited by dendritic cell-based vaccines in association with enhanced therapeutic efficacy. Cancer Res 2002;62:5853–8.
12. Vidal-Vanaclocha F, Fantuzzi G, Mendoza L, et al. IL-18 regulates IL-1β-dependent hepatic melanoma metastasis via vascular cell adhesion molecule-1. Proc Natl Acad Sci U S A 2000;97:734–9.
13. Cho D, Song H, Kim YM, et al. Endogenous interleukin-18 modulates immune escape of murine melanoma cells by regulating the expression of Fas ligand and reactive oxygen intermediates. Cancer Res 2000;60:2703–9.
14. Park CC, Morel JC, Amin MA, Connors MA, Harlow LA, Koch AE. Evidence of IL-18 as a novel angiogenic mediator. J Immunol 2001;167:1644–53.
15. Dinarello CA. Targeting interleukin 18 with interleukin 18 binding protein. Ann Rheum Dis 2000;59 Suppl 1:i17–20.
16. Faggioni R, Cattley RC, Guo J, et al. IL-18-binding protein protects against lipopolysaccharide- induced lethality and prevents the development of Fas/Fas ligand-mediated models of liver disease in mice. J Immunol 2001;167:5913–20.
17. Sivakumar PV, Westrich GM, Kanaly S, et al. Interleukin 18 is a primary mediator of the inflammation associated with dextran sulphate sodium induced colitis: blocking interleukin 18 attenuates intestinal damage. Gut 2002;50:812–20.
18. Nicoletti F, Di Marco R, Papaccio G, et al. Essential pathogenic role of endogenous IL-18 in murine diabetes induced by multiple low doses of streptozotocin. Prevention of hyperglycemia and insulitis by a recombinant IL-18-binding protein: Fc construct. Eur J Immunol 2003;33:2278–86.
19. Mankoff DA. A definition of molecular imaging. J Nucl Med 2007;48:18N, 21N.
20. Cherry SR, Shao Y, Silverman RW, et al. MicroPET: a high resolution PET scanner for imaging small animals. IEEE Trans Nucl Sci 1997;44:1161–6.
21. Paulus MJ, Gleason SS, Kennel SJ, Hunsicker PR, Johnson DK. High resolution X-ray computed tomography: an emerging tool for small animal cancer research. Neoplasia 2000;2:62–70.
22. Hwang JY, Moffatt-Blue C, Equils O, et al. Multimode optical imaging of small animals: development and applications. Proc SPIE 2007;6441:644105/1-/10.
23. Cai W, Rao J, Gambhir SS, Chen X. How molecular imaging is speeding up anti-angiogenic drug development. Mol Cancer Ther 2006;5:2624–33.
24. Massoud TF, Gambhir SS. Molecular imaging in living subjects: seeing fundamental biological processes in a new light. Genes Dev 2003;17:545–80.
25. Cai W, Chen K, Mohamedali KA, et al. PET of vascular endothelial growth factor receptor expression. J Nucl Med 2006;47:2048–56.
26. Cai W, Wu Y, Chen K, Cao Q, Tice DA, Chen X. *In vitro* and *in vivo* characterization of 64Cu-labeled AbegrinTM, a humanized monoclonal antibody against integrin avb3. Cancer Res 2006;66:9673–81.
27. Cai W, Ebrahimnejad A, Chen K, et al. Quantitative radioimmunoPET imaging of EphA2 in tumour-bearing mice. Eur J Nucl Med Mol Imaging 2007;34:2024–36.
28. Cai W, Olafsen T, Zhang X, et al. PET imaging of colorectal cancer in xenograft-bearing mice by use of an 18F-labeled T84.66 anti-carcinoembryonic antigen diabody. J Nucl Med 2007;48:304–10.
29. Randle JC, Harding MW, Ku G, Schonharting M, Kurrle R. ICE/Caspase-1 inhibitors as novel anti-inflammatory drugs. Expert Opin Investig Drugs 2001;10:1207–9.
30. Siegmund B. Interleukin-1β converting enzyme (caspase-1) in intestinal inflammation. Biochem Pharmacol 2002;64:1–8.
31. Jenkins DE, Oei Y, Hornig YS, et al. Bioluminescent imaging (BLI) to improve and refine traditional murine models of tumor growth and metastasis. Clin Exp Metastasis 2003;20:733–44.
32. Szentirmai O, Baker CH, Lin N, et al. Noninvasive bioluminescence imaging of luciferase expressing intracranial U87 xenografts: correlation with magnetic resonance imaging determined tumor volume and longitudinal use in assessing tumor growth and anti-angiogenic treatment effect. Neurosurgery 2006;58:365–72.
33. Hsu AR, Hou LC, Veeravagu A, Tse V, Chen X. *In vivo* near-infrared fluorescence imaging of integrin avb3 in an orthotopic glioblastoma model. Mol Imaging Biol 2006;8:315–23.
34. Gambhir SS, Czernin J, Schwimmer J, Silverman DH, Coleman RE, Phelps ME. A tabulated summary of the FDG PET literature. J Nucl Med 2001;42:1–93S.
35. Frese KK, Tuveson DA. Maximizing mouse cancer models. Nat Rev Cancer 2007;7:645–58.
36. Weigelt B, Peterse JL, van 't Veer LJ. Breast cancer metastasis: markers and models. Nat Rev Cancer 2005;5:591–602.
37. Mehlen P, Puisieux A. Metastasis: a question of life or death. Nat Rev Cancer 2006;6:449–58.
38. Gwyther SJ. New imaging techniques in cancer management. Ann Oncol 2005;16 Suppl 2:ii63–70.
39. Rudin M, Weissleder R. Molecular imaging in drug discovery and development. Nat Rev Drug Discov 2003;2:123–31.
40. Carrascal MT, Mendoza L, Valcárcel M, et al. Interleukin-18 binding protein reduces b16 melanoma hepatic metastasis by neutralizing adhesiveness and growth factors of sinusoidal endothelium. Cancer Res 2003;63:491–7.